Article

The East Variscan Shear Zone (EVSZ) and Its Regional Mylonitic Complex: A New Geodynamic Interpretation of the Variscan Axial Zone in Sardinia (Italy)?

Federico Mantovani [ID] and Franco Marco Elter *[ID]

Department of Earth, Environment and Life Science (DISTAV), University of Genova, 16132 Genova, Italy;
federico.mantovani@edu.unige.it
* Correspondence: franco.elter@unige.it

Abstract: Sardinia (Italy) represents one of the most comprehensive cross-sections of the Variscan orogen. The metamorphic and structural complexity characterizing its axial zone still presents many unresolved issues in the current state of knowledge. The data presented from the structural study of the entire axial zone of this area have allowed the authors to propose a subdivision into two new structural complexes. In particular, a younger complex is identified as the New Gneiss Complex, containing remnants of an older and higher-grade metamorphic complex defined as the Old Gneiss Complex. The structural and geometric relationships between the two complexes suggest the redefinition of the axial zone of Sardinia as part of the intracontinental East Variscan Shear Zone/medium-temperature Regional Mylonitic Complex. Comparable relationships are also highlighted in many other areas of the Variscan chain (e.g., Morocco, Corsica, Maures Massif, and Argentera Massif). Extending this new structural interpretation to other axial zones of the South European Variscan orogen could provide new hints for reconstructing the collision boundaries between Gondwana and Laurussia in the late Carboniferous to the early Permian periods.

Keywords: Variscan; Sardinia; shear zone; EVSZ; Mylonitic Complex; Carboniferous; Permian

1. Introduction

The Devonian–Carboniferous European Variscan Belt, or Variscides, formed due to the convergence between Laurussia to the north and Gondwana to the south (in present-day orientation). This convergence led to the closure of intermediate oceanic basins and the accretion of diverse terranes [1–11]. The geodynamic evolution of the Variscides and its geological implications can be summarized as follows: (i) during the Devonian to early Carboniferous periods, subduction and collision events occurred, leading to the stacking of nappes and subsequent thickening of the crust; (ii) in the late Carboniferous to early Permian periods, dextral wrenching ensued following oblique convergence between Gondwana and Laurussia, resulting in the reactivation or formation of large-scale strike–slip faults and shear zones within the crust, the emplacement of significant volumes of granitoids, and the formation of narrow intracontinental basins accompanied by bimodal magmatism; and (iii) during the middle Permian period, a generalized tectonic setting prevailed, which led to the development of gradually expanding sedimentary basins marking the onset of the Alpine sedimentary cycle.

The geology of the Variscan Belt in western and central Europe is characterized by four NE–SW-trending tectonic zones [8,12–14]. These zones represent ribbon continents that underwent various degrees of reworking during the protracted Palaeozoic evolution of the Variscan orogenic system. Although this zonal structure appears linear, it is not entirely cylindrical, and it is further compartmentalized into three distinct domains separated by regional transcurrent faults (Figure 1), each exhibiting differences in geodynamic evolution: (i) the Northern Variscan Domain (NVD), which includes the Bohemian Massif,

Schwartzwald, and Vosges basement outcrops; (ii) the Central Variscan Domain (CVD), which encompasses the French Massif Central, Armorican Massif, and SW England; and (iii) the southern Variscan domain (SVD), which features the geology of the Iberian Peninsula and the Sardinia–Corsica–Maures/Tanneron block [8,12–14]. In the SVD, however, Refs. [8,11,15] do not consider other Variscan areas, such as the Variscan massifs of Calabria, the Ligurian–Maritime–Western Alps, and the basement of the Northern Apennines (GDC, Gondwana-Derived Continents [6,7,9,16–19]). The NVD is separated from the CVD by the Pays de Bray Shear Zone (PBSZ), and the CVD is delimited from the SVD by the South Armorican Shear Zone (SASZ) [8], while the East Variscan Shear Zone (EVSZ [6,7,9,20]) represents the southernmost margin between the GDC (to the south) and Gondwana (to the north). The collision between Gondwana and Laurussia involved large continental masses and several Gondwana-derived microcontinents [4,20–22]. The irregular boundaries of the colliding microplates caused coeval transpressional and transtensional tectonics, along with a complicated pattern of intracontinental shear zones at the scale of the southern European Variscides [9,22–27].
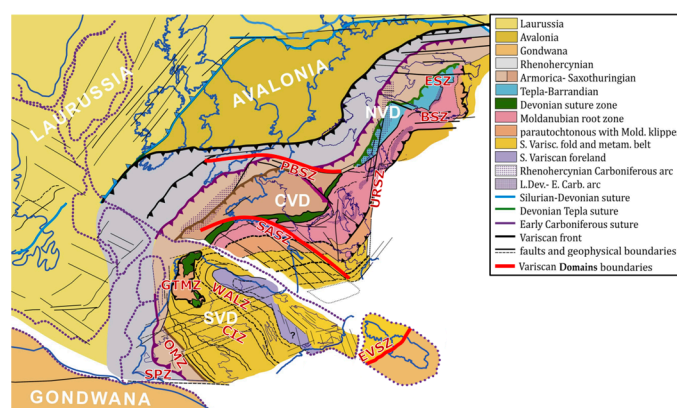

Figure 1. Geological map showing a hypothetical reconstruction of the Variscan Belt in the Middle Triassic. NVD: North Variscan Domain; CVD: Central Variscan Domain; SVD: South Variscan Domain; BSZ: Elbe Shear Zone; CIZ: Central Iberia Zone; EVSZ: East Variscan Shear Zone; OMZ: Ossa-Morena Zone; PBSZ: Pays de Bray Shear Zone; RSZ: Rhinegraben Shear Zone; SASZ: South Armorican Shear Zone; SPZ: South Portuguese Zone; SSZ: Sudetian Shear Zone; TMZ: Galicia-Tras-os-Montanes Zone; WALZ: West Asturian-Leonese Zone (modified from [8]).

In Sardinia, the East Variscan Shear Zone (EVSZ) is located in the Axial Zone. Studies conducted over the years on the High-Grade Metamorphic Complex (HGMC) have only considered certain outcrops (e.g., the San Teodoro coast, Monte Plebi, and some outcrops along the Punta Bados–Morungiu Nieddu coast). However, ref. [28] highlighted the presence of lithtypes composed of high-grade metamorphic rocks (granulitic and amphibolitic facies) embedded within a peculiar milonitic lithology of a lower grade (greenschist) in the coastal stretch between Olbia-Pittulongu and Golfo Aranci and in the Barrabisa area.

Through the structural analysis of the data collected for this paper, the authors aim to delineate the relationships among the aforementioned lithologies outcropping along the East Variscan Shear Zone and the Axial Zone of Sardinia. Furthermore, the obtained results are compared with other neighboring Variscan areas in order to identify possible regional-scale correlations.

2. Materials and Methods

A structural analysis was conducted at twenty-two locations (Figure 2) where high-temperature (HT) lithotypes were exposed. This survey involved identifying and measuring various structural elements, both planar and linear, and analyzing their geometric relationships. Subsequently, statistical data from the poles of identified planar surfaces (695 measurements) and coeval linear elements (441 measurements) were processed using the "Stereonet" software by Richard W. Allmendinger © 2020–2022 v. 11.5.4. Linear

elements were categorized based on the mineralogical species involved in the tectonic process. Once mineralogical lineations were identified, observable kinematic indicators were determined and classified on the XZ plane to define the sense of shear associated with the two deformation events. The geological maps and sketches were produced with "QGis™" software v. 3.28.11, "Inkscape: Open Source Scalable Vector Graphics Editor™" v. 1.3, and "Vectary™" software v. 3.0.
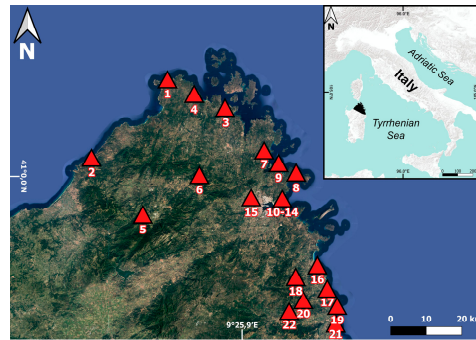

Figure 2. Satellite view of the studied area (highlighted in black in the geographic inset); red triangles indicate the locations where data were collected. 1: P.ta Falcone; 2: Trinità d'Agultu; 3: Palau; 4: Capo ferro-Cala Grande; 5: Tempio Pausania; 6: Diga del Liscia; 7: Golfo di Cugnaga; 8: Golfo Aranci; 9: Cala Libeccio-Golfo Marinella; 10: P.ta Bados; 11: Cala Banana; 12: Nodu e Pianu; 13: Morungiu Nieddu-Sos Aranzos; 14: Pittolongu; 15: Olbia-M.te Plebi; 16: S. Teodoro; 17: Budoni; 18: P.ta Tittinosu-P.ta de li Tulchi; 19: P.ta Ainu; 20: Brunella-S. Lorenzo; 21: P.ta Orvili-M.te Longu; 22: P.ta Nidu e Corvu-Posada Valley.

3. Geological Framework of Sardinia

The Variscan basement of Sardinia has been divided into four NW–SE-trending tectono-metamorphic zones [28–30], with a notable increase in metamorphic grade from the SW to the NE [31]. Moving from SW to NE, these zones are the External Zone (foreland), the Nappe Zone (further divided into External and Internal Nappe Zone), the Posada Valley Shear Zone (PVSZ) or Posada–Asinara Line, and the Axial Zone or High-Grade Meta-morphic Complex (HGMC), which outcrops in the northern part of the island (Figure 3).
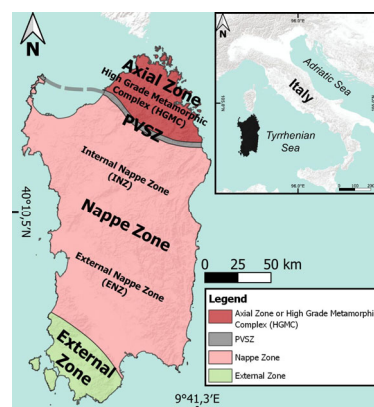
Figure 3. The Variscan Belt in Sardinia and its zones.

The External Zone represents the foreland of the chain and primarily includes Cambrian–Early Ordovician terrigenous sequences and platform carbonate successions. The Nappe Zone consists of Cambrian–Early Ordovician metasedimentary and Ordovician metavolcanic rocks, which are stacked in an NW–SE-trending nappe with a main vergence toward the SW [32], resulting from an NW–SE trending thrust [33]. Ref. [28] attribute the formation of these nappes to the collision between Gondwana and Laurussia. The Posada Valley Shear Zone (PVSZ) or Posada–Asinara Line [34–37] has been interpreted by [38,39]

as a Condensed Isogrades Zone, exhibiting a sharp increase in metamorphic grade from SW to NE within a narrow band. The HGMC comprises HT rocks ranging from granulitic to green-schist facies conditions [31,40].

The Variscan Shear Zones in Sardinia

Since 1990, shear zones have been reported at a regional scale in the Variscan orogeny, such as the Grighini Shear Zone, the Posada Valley Shear Zone, and the East Variscan Shear Zone [6,7,9,28,38,41–44], which are recognizable in the Internal Nappe Zone (the first one) and in the High-Grade Metamorphic Complex (HGMC).

The East Variscan Shear Zone (EVSZ [6,7,9,20,45,46]) was a Variscan intracontinental dextral strike–slip shear zone whose remnants may be found from Slovenia across the Alps to North Africa. Active between 325 ± 1.3 Ma and 315 ± 1.3 Ma [6,36,47], the EVSZ was temporally and spatially connected with the Atlas Shear System and the Elbe Shear Zone. Its width varies from a few kilometers (e.g., Emosson Lake, Aiguilles Rouges-Mt. Blanc massifs in [48], and in the Argentera Massif in [49]) to 90 km (Sardinian Massif in [7,9,28]. The geological evolution of the EVSZ locally reveals a complex history.

4. Geological Framework of the High-Grade Metamorphic Complex (HGMC)

The High-Grade Metamorphic Complex (HGMC) of the Sardinian basement is characterized by the highest degree of metamorphism, ranging from high amphibolite to granulite facies conditions, extending from southwest to northeast [31,50]. Ref. [9] outline that the HGMC comprises two gneiss complexes primarily exhibiting amphibolite facies conditions (344 Ma [38,51]): the Old Gneiss Complex (OGC) and the New Gneiss Complex (NGC). The OGC consists of ortho/paragneiss trending NE–SW, along with subordinate migmatitic gneiss containing a low percentage of centimeter-sized stromatic leucosomes (approximately 3–5% [40]), orthoderivates, and metabasites (amphibolitized granulites, eclogites, and amphibolites sensu strictu). On the other hand, the NGC represents a retrograde NW–SE mylonitic gneiss complex (referred to as the Cat's Eyes Facies, CEF [28]), featuring syn-tectonic intrusions of granites dated at approximately 318 ± 3 Ma to 316 ± 2 Ma [7].

Structural and Metamorphic Frame of the High-Grade Metamorphic Complex (HGMC)

Ref. [28] highlighted that the High-Grade Metamorphic Complex (HGMC) is characterized by five deformational events (D) and three metamorphic events (M): in their geometrical order of superposition, they are D2 (syn-tectonic with M2), D2a, D3 (syn-tectonic with M3), D4 (syn-tectonic with M4), and D5. The D2 event is marked by the syn-kinematic S2 foliation developed at P-T conditions of granulite facies (M2, 650–750 °C and 8–12 Kb at 352 ± 3 Ma [52,53]). Rare Fsp σ-porphyroclasts and asymmetric boudins show a top-to-the-NW component of shear. The D2a is distinguished solely by infrequent tight folds and no metamorphic imprint. The D3 event produced the main NE–SW pervasive regional foliation (S3) developed under amphibolite facies (M3, 550–740 °C and 3–7 Kb at 344 ± 7 Ma [31,51]). The D3 event defines a shear-parallel foliation and a transverse lineation. σ-type mantled/δ-type mantled porphyroclasts and stepped fragmented grains [54,55] consistent with a top-to-SE component of shear are recognizable. The D4 event is coeval with a greenschist to sub-greenschist stage (M4, 300–400 °C and 2–3 Kb [31] at 300 Ma [56]) and associated with the development of metric to kilometric dextral shear zones, which are characterized by mylonitic foliation (S4) and an NW–SE-oriented Bt-Ms lineation. S–C planes, mantled porphyroclasts of Fsp and Qz, centimeter- to kilometer-sized sigmoidal gneissic pods, syn-shearing folds, and drag folds indicate an NW–SE dextral sense of shear. The D5 event marks the last deformational phase, and it is not accompanied by a distinct metamorphic episode. It is characterized by numerous folds of varying morphological types, with NE–SW and NW–SE axes (Table 1).

Table 1. Relationships between high-temperature (HT) metamorphic events and deformational phases described by [28,53,57–61].

D2	M2	Granulite stage (650–750 °C; 8–12 Kb at 352 ± 3 Ma)	Isolated relics of metamorphic banding (S2) within the Ky-bearing gneiss and granulites. Rare kinematic indicators show a top-to-NW component of shear.
D2a	-	-	Intertectonic associated with rare, tight folds, which deformed the S2 foliation only in quartzitic nodules.
D3	M3	Amphibolite stage (550–740 °C; 3–7 Kb at 344 ± 7 Ma)	Strain facies shear-parallel foliation (S3) and shear-parallel lineation (ab-foliation/a-lineation). NW–SE mineral lineations defined by rods/pencils of Pl and Qz, as well as Sil and Ms. Kinematic indicators with top-to-SE component of shear.
D4	M4	Greenschist to sub-greenschist stage (300–400 °C; 2–3 Kb at 300 Ma)	Ab-shear-parallel foliation (S4) and a-shear-parallel mineral lineation. Kinematic indicators, consistent with an NW–SE dextral sense of shear. Coeval emplacement of the Barrabisa NW–SE syn-tectonic granite.
D5	-	-	Several folds of different morphological types, with NE–SW and NW–SE axes.

However, over the past 13 years, new structural data have been acquired and collected in several new areas of the HGMC by the authors of this paper. These new data have made it possible to simplify and provide a new interpretation of the HGMC's structural features (Table 2). The new structural framework of the HGMC is characterized, in their geometrical order of superposition, by three deformational events: D2 (syn-tectonic with M2), recognizable in the Old Gneiss Complex (OGC; D2+D3 in [28,62]); D3 (syn-tectonic with M3), recognizable in the New Gneiss Complex (NGC; D4 in [28]); and the latest D4 (D5 [28]). Given the aim of this paper (to define the relationships between OGC and NGC) and considering that the datings of the granulitic and amphibolitic events fall within the same time interval (approximately 350–344 million years ago) and no geometric overlaps between these two metamorphic events are observed, we prefer to simplify by merging the D2 and D3 events in [28] into a single event (referred to as D2 in this paper). This simplification was also previously proposed by [31].

Table 2. Comparison of the relationships between high-temperature (HT) metamorphic events and deformational phases in [28] and in this paper.

Elter et al., 2010 [28]			This Paper		
D2	M2	Granulite stage (650–750 °C; 8–12 Kb at 352 ± 3 Ma)	D2	M2	Granulite stage (650–750 °C; 8–12 Kb at 352 ± 3 Ma) followed by amphibolite stage (550–740 °C; 3–7 Kb at 344 ± 7 Ma)
D2a	-	-			
D3	M3	Amphibolite stage 550–740 °C; 3–7 Kb a7 344 ± 7 Ma)			
D4	M4	Greenschist stage (300–400 °C; 2–3 Kb at 300 Ma)	D3	M3	Greenschist stage (300–400 °C; 2–3 Kb)
D5	-	-	D4	-	-

5. Results

Data collection encompassed 22 distinct localities, each representing areas where tectonometamorphic events impacted the High-Grade Metamorphic Complex (HGMC). The collected data will be presented separately and organized by geological complex, thereby reflecting the specific tectonometamorphic event under investigation. This method of categorization ensures a focused analysis of the geological processes within each complex, offering insights into the diverse mechanisms propelling tectonometamorphism across the study area. By structuring the results in this manner, our goal is to delineate the nuanced

variations in tectonic and metamorphic histories within and among geological complexes, thereby fostering a comprehensive comprehension of the regional geological evolution.

5.1. The Old Gneiss Complex (OGC)

The Old Gneiss Complex (OGC) comprises a diverse array of lithotypes (Figure 4), including orthoderivates (Figure 4a,b), paraderivates (Figure 4c–e), rare marbles (Figure 4f), metabasites (Figure 4g,h), and subordinate stromatitic gneisses (Figure 4i–k).
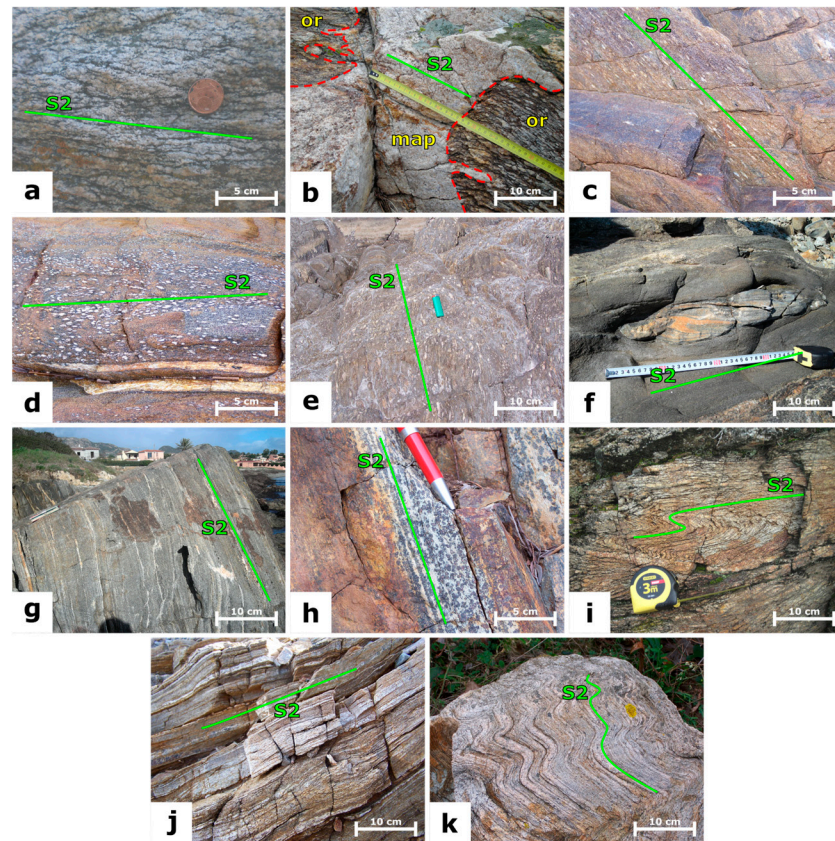

Figure 4. Lithotypes of the OGC; (**a**) Punta Pedrami: orthogneiss (seen from NW); (**b**) Golfo Aranci: Ordovician relationships between meta-aplite dike (map) and orthogneiss (or) where the primary contact (red dotted line) is crosscut by S2 (seen from SW); (**c**) Capo Ferro: Sil-bearing gneiss (seen from SE); (**d**) Punta Bados: Sil-bearing gneiss (seen from SE); (**e**) Punta dell'Ainu: Sil-bearing gneiss (seen from NW); (**f**) Punta Batteria: deformed calsilicate boudin in biotitic gneiss (seen from NW); (**g**) Pittolongu: decametric pod of amphibolite embedded in the NGC (seen from S); (**h**) Punta de li Tulchi: amphibolitized eclogite (seen from SE); (**i**) Trinità d'Agulto: folded stromatitic gneiss (seen from N); (**j**) Cala Finocchio-San Teodoro: stromatitic gneiss (seen from SE); (**k**) Punta de li Tulchi: folded stromatitic gneiss (seen from NE).

Within these lithotypes, the percentage of leucosomes has been estimated at approximately 3% and 5% in the orthoderivates and paraderivates, respectively. The structural framework of the OGC is characterized by a notable deformational event (D2), which is identifiable within these lithotypes. The syn-tectonic M2 metamorphic event is constrained between the Granulite stage (650–750 °C and 8–12 kbar [31]), dated at 359 ± 4 Ma [7], and the Amphibolite stage (550–740 °C and 3–7 kbar), at around 350–344 Ma ± 7 Ma [31], developing a pervasive regional S2 foliation consistently aligned with an NE–SW direction, with a notable inclination towards SE (Figure 5a).
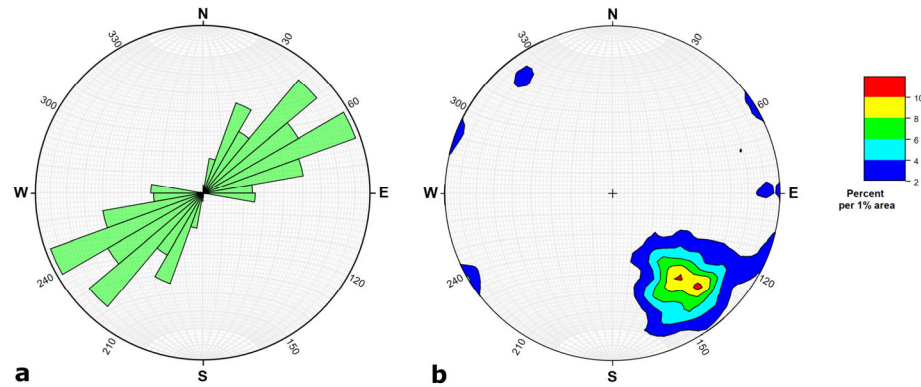
Figure 5. (**a**) Rose diagram of 305 S2 planes in the OGC (equal area, lower hemisphere). (**b**) Poles of 325 mineralogical lineation (L2) on the S2 surface in the OGC.

Measurements pertaining to mineralogical lineations (L2) identified on the S2 surface were categorized based on the involved mineralogical species, including lineations composed of a combination of Bt and Ms (Figure 6a), rods/pencils of Qz and Kfs (Figure 6b), Amp (Figure 6c), and Sil (Figure 6d).
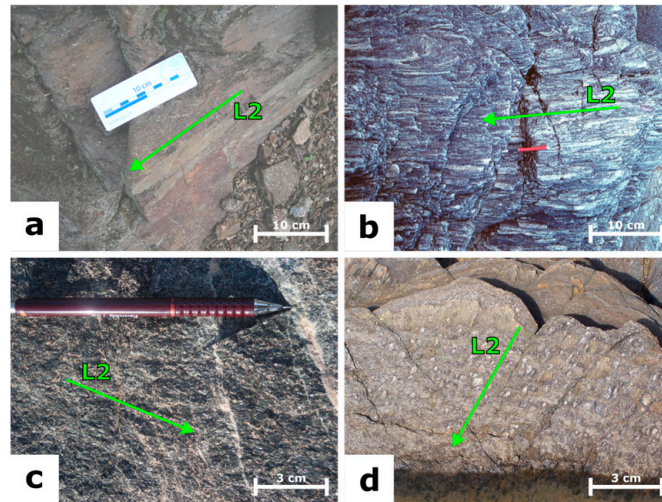

Figure 6. Mineralogical lineations (L2) on the S2 surface of OGC; (**a**) Trinità d'Agultu: Ms + Bt (seen from NE, XY plane); (**b**) Golfo Aranci: rods of Kfs (seen from SW, XY plane); (**c**) Morungiu Nieddu: Hbl (seen from NW, XY plane); (**d**) Punta dell'Ainu: Sil + Ms (seen from NE, XY plane).

These mineralogical lineations exhibit varying inclinations ranging from vertical to oblique. The trends observed in all areas reveal a consistent NW–SE orientation across mineralogical species, with a general dip towards SE (Figure 5b).

Associated kinematic indicators on the XZ plane, such as σ-type mantled/δ-type mantled porphyroclasts and stepped fragmented grains, are also present, indicating a regional top-to-the-SE component of shear (Figure 7).

The application of strain facies to the D2 structures, utilizing the Flinn diagram for Sil + Ms, reveals the occurrence of both oblate and prolate Sil + Ms ellipsoids [28]. Additionally, a kinematic vorticity analysis of the calcsilicate nodules indicates a general shear deformation with pure shear dominating over simple shear [28]. These S2 strain features enable the definition of an overall transpressional kinematics.
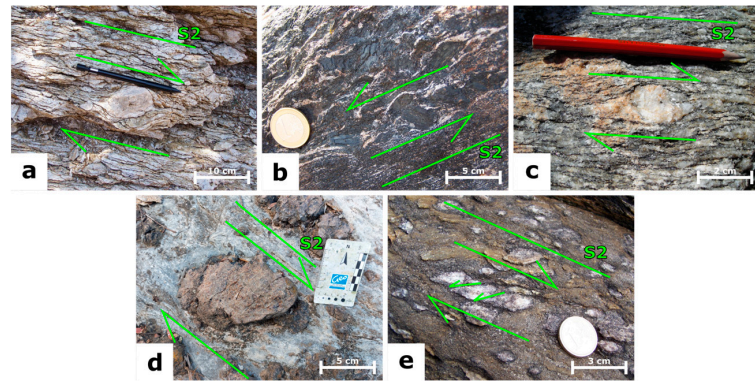
Figure 7. Kinematic indicators related to S2 [55,63] of the OGC; (**a**) Golfo Aranci: top-to-right (SE) Kfs σ-type porphyroclasts (seen from SW, XZ plane); (**b**) Morungiu Nieddu: top-to-left (SE) Hbl σ-type porphyroclasts with Pl (seen from NE); (**c**) Punta de li Tulchi: top-to-right (SE) Kfs σ-type porphyroclast (seen from SW, XZ plane); (**d**) Tamarispa: Grs top-to-right (SE) σ-type porphyroclast (seen from SW, XZ plane); (**e**) Punta dell'Ainu: top-to-right (SE) top-to-right (SE) domino-like Sil + Ms object (seen from SW, XZ plane).

5.2. The New Gneiss Complex (NGC)

The New Gneiss Complex (NGC) is primarily characterized by the presence of Bt-bearing mylonitic gneisses (Cat's Eyes Facies, CEF, in [28]) alongside syn-tectonic per-aluminous granites (Figure 8a). Within the NGC, these Bt-bearing gneisses exhibit a distinctive augen structure marked by the occurrence of millimetric to decimetric porphyroclasts, contributing to their unique appearance and texture (Figure 8a–k). Moreover, scattered throughout the NGC are pods of various sizes, ranging from centimeters to decameters, comprising lithotypes associated with the Old Gneiss Complex (OGC), including but not limited to amphibolitized eclogites, amphibolites, orthogneiss, quartzites, and calcsilicate nodules. This intermingling of lithotypes from the OGC within the NGC adds to the complexity and heterogeneity of the geological setting.
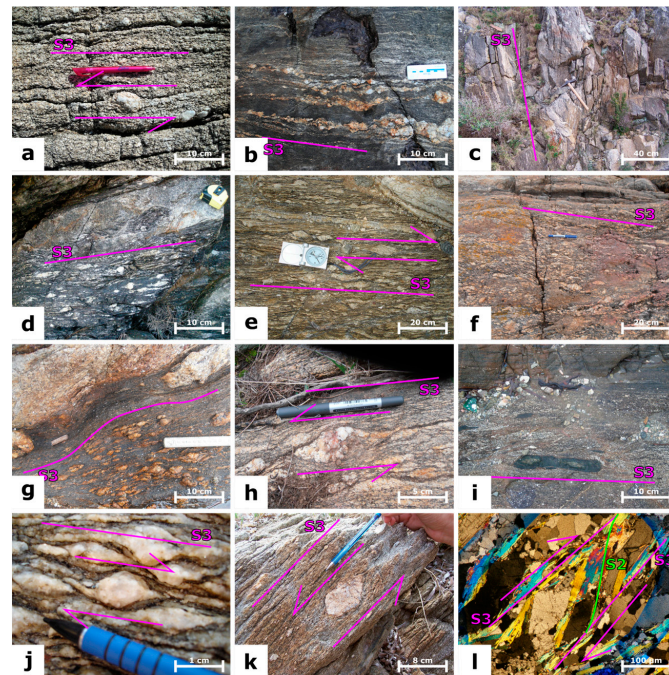

Figure 8. Lithotypes of the NGC; (**a**) Cala Spada: syn-tectonic D3 granitoid with top-to-left (NW) σ-type Kfs porphyroclasts (seen from SW, XZ plane); (**b**) Isola dei Gabbiani: sigmoidal Qz that acts

as ductile shear S-fabric revealing a top-to-right (SW) shear (seen from NW, XZ plane); (**c**) Serra Tamburo: (seen from NW); (**d**) Capo Ferro: sigmoidal/pull-apart Qz aggregates that act as ductile shear S-fabric reveal a top-to-right (NW) shear (seen from NE, XZ plane); (**e**) Cala Moresca: mylonitic orthogneiss with ductile S3 sheared foliation with top-to-right (SE) σ-type Kfs porphyroclasts (seen from SW, XZ plane); (**f**) Cala Libeccio: mylonitized and ultramylonitized Bt-bearing gneiss (fine band) with train of interconnected sigmoidal Qz pods (seen from N, XZ plane); (**g**) Punta Bados: mylonitic Bt-bearing gneiss with train of interconnected sigmoidal-shaped Qz pods (seen from SW, XZ plane); (**h**) Nodu e Piano: mylonitic Bt-bearing gneiss with top-to-left (NW) ductile sheared Qz pod (seen from SW, XZ plane); (**i**) Pittolongu: ultamylonite with centimetric amphibolite pods (green/black) embedded in wavy S3 (seen from SW, XZ plane); (**j**) Sos Aranzos: mylonitized orthogneiss with top-to-right (SE) ductile shear δ-type Kfs porphyroclasts (seen from SW, XZ plane); (**k**) Punta Orvili: mylonitic Bt-bearing gneiss with top-to-left (NW) ductile sheared Qz clast (seen from SW, XZ plane); (**l**) Capo Ferro: top-to-right (SE) ductile shear S-C planes in thin section of mylonitic Bt-bearing gneiss with S2 and S3 relationships (oriented sample seen from SW, XZ plane, crossed polar, X10).

The D3 event is prominently observed within the NGC. This event occurs concurrently with the emplacement of both the NW–SE-oriented Capo Ferro syn-tectonic Barrabisa granite, precisely dated at 325 ± 1.3 Ma [7], and the Cala Spada syn-tectonic granite (Figure 8a) for which datations are currently unavailable. The syn-kinematic M3 metamorphic event associated with the D3 event corresponds to the greenschist stage (Figure 8l, 300–400 °C and 2–3 kbar [7]), resulting in the development of a pervasive schistosity (S3). This schistosity (S3), often displaying a mylonitic character, is associated with a Bt + Ms lineation (L3), both of which exhibit an NW–SE orientation (Figure 9). Across different areas, the trend of S3 consistently aligns in an NW–SE direction (Figure 9a), with steep inclinations towards both SW and NE. Detailed measurements conducted on mineralogical lineations (L3) identified on the S3 surface, primarily composed of Bt + Ms, reveal a prevailing NW–SE trend with inclinations predominantly towards the SE (Figure 9b). Considering their inclination, these mineralogical lineations can be categorized as oblique lineations.
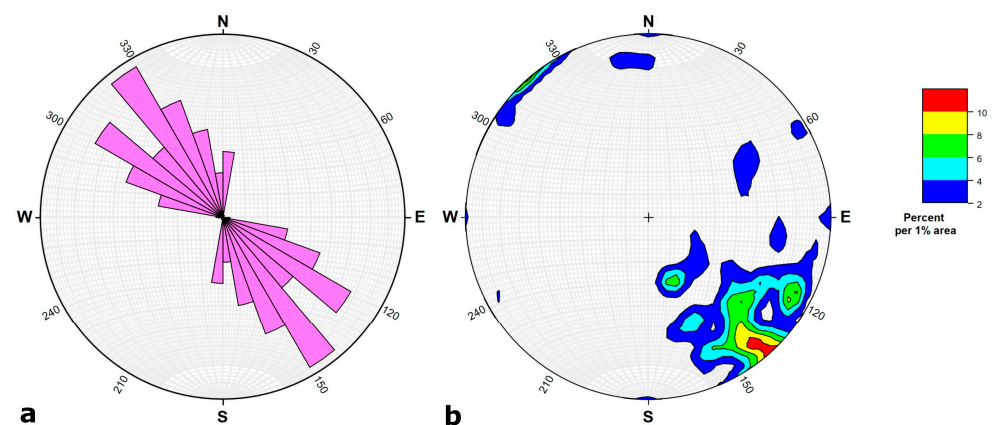

Figure 9. (**a**) Rose diagram of 390 S3 planes in the NGC (equal area, lower hemisphere). (**b**) Poles of 116 mineralogical lineation (L3) on the S3 surface in the NGC.

On the XZ plane of the S3 foliation, various kinematic indicators are readily observable, providing valuable insights into the deformation history. These indicators include well-defined S-C planes (Figure 10a), distinctive domino-like porphyroclasts (Figure 10b), δ-type porphyroclasts (Figures 8j and 10c), σ-type porphyroclasts (Figure 8a,e and Figure 10c), asymmetric calcsilicate boudins, as well as centimeter- to kilometer-scale sigmoidal gneissic pods (Figure 10d). Moreover, the presence of tension gashes (Figure 10e), syn-shearing folds, and drag folds further underscores the complexity of the deformation processes involved. The observed shear features exhibit a regional dextral sense of shear. In the Capo Ferro, Sos Aranzos, and Punta de li Tulchi areas, a local sinistral sense of shear is also recognizable. Both senses of shear are aligned in an NW–SE orientation.
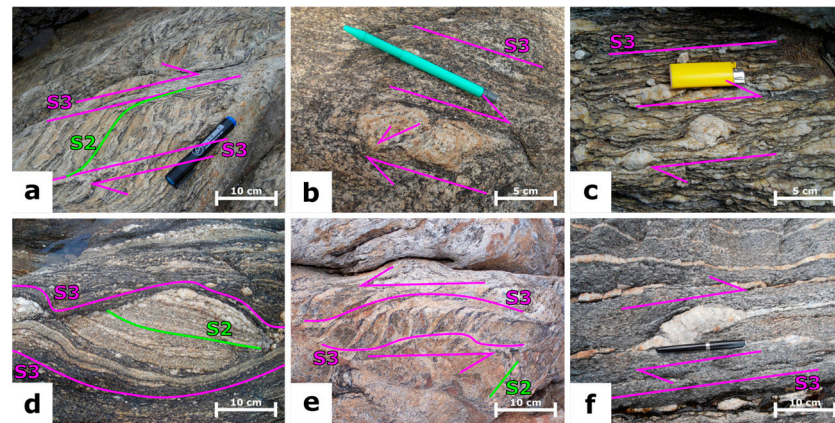
Figure 10. Kinematic indicators related to S3 [55,63] of the NGC; (**a**) Capo Ferro: top-to-right (NE) S–C planes (seen from SE, XZ plane); (**b**) Cala Banana: top-to-right (SE) domino-like Qz object (seen from SW, XZ plane); (**c**) Cala Moresca: top-to-right (SE) δ-type Kfs porphyroclast (seen from SW, XZ plane); (**d**) Pittolongu: top-to-right (SE) ductile sheared decimetric pod of OGC (seen from SW, XZ plane); (**e**) Punta de li Tulchi: top-to-left (NE) tension gashes filled by leucosome related to a sinistral sense of shear (seen from NW, XZ plane); (**f**) Cala Serenella: top-to-right sigmoidal/parallelogram rootless Qz vein (seen from NW, XZ plane).

5.3. Relationships between the Old Gneiss Complex (OGC), the New Gneiss Complex (NGC), and the Posada Valley Shear Zone (PVSZ)

The relationships between the Old Gneiss Complex (OGC) and the New Gneiss Complex (NGC) constitute a significant aspect of the geological dynamics within the High-Grade Metamorphic Complex (HGMC) of northeastern Sardinia. These are prominently displayed across various outcrops (Figure 11) in which pods spanning a range of scales from decimetric to decametric dimensions are present. These pods consist of a diverse array of lithotypes, encompassing amphibolitized eclogites, amphibolites, orthogneiss, quartzites, and calcsilicate nodules. Within these pods, evidence of the S2 foliation attributed to the D2 event that characterizes the OGC is discernible, allowing the author to hypothesize them as fragments of OGC lithotypes embedded in the NGC ones. The S2 foliation may exhibit deformation through folds lacking axial surface schistosity.
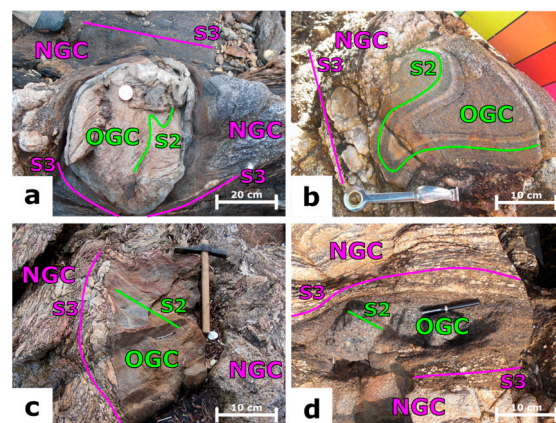
Figure 11. Examples of the relationships between OGC and NGC; (**a**) Punta Bados: OGC calcsilicates pod with relics of folded S2 embedded in the NGC (seen from NE); (**b**) Punta Serenella: OGC quartzite pod with deformed S2 (seen from NE); (**c**) Sos Aranzos: decametric amphibolite pod with S2 foliation embedded in the NGC (seen from NW); (**d**) Cala Libeccio: amphibolitized eclogite embedded in the OGC (seen from S).

Furthermore, the interplay between the NW–SE-oriented D3 event in the NGC and the dextral E–W Posada Valley Shear Zone (PVSZ [41,64,65]) is primarily observed only in

the Punta Orvili area. Situated in close proximity to the Posada Valley, the Punta Orvili area represents the southernmost outcrop of the HT lithotypes. Here, the NW–SE-oriented S3 foliation intersects with the E–W-oriented dextral shear zones system of the PVSZ. Characterized by slender green shear zones with thicknesses ranging from 2 to 10 cm, the PVSZ delineates a Riedel system indicative of a dextral sense of shear (Figure 12).
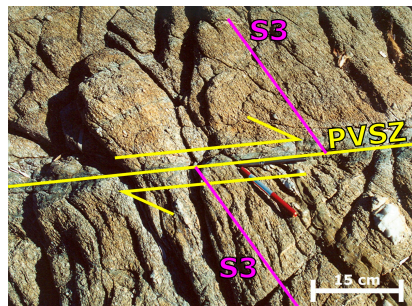

Figure 12. Punta Orvili: relationships between NGC and PVSZ (seen from N).

6. Discussion

In Table 3, we have summarized the chronological framework of events that affected the High-Grade Metamorphic Complex (HGMC), utilizing data collected in this paper as well as literature sources.

Table 3. Potential chronological framework of events that affected the High-Grade Metamorphic Complex (HGMC).

Age	Tectonic Frame	Magmatism	Metamorphism	Planar Anisotropy	P-T Condition
290	-	Emplacement of calc-alkaline granitoid suite	-	-	-
300	PVSZ (dextral strike–slip top to E)	Emplacement of calc-alkaline granitoid suite	Greenschist stage	Sm in the PVSZ	300–400 °C; 2–3 Kb
310	PVSZ (dextral strike–slip top to E)	Emplacement of calc-alkaline granitoid suite	Greenschist stage	Sm in the PVSZ	300–400 °C; 2–3 Kb
315	EVSZ (dextral strike–slip top to SE)	Capo Ferro Granite	Greenschist stage	S3	300–400 °C; 2–3 Kb
320	EVSZ (dextral strike–slip top to SE)	Capo Ferro Granite	Greenschist stage	S3	300–400 °C; 2–3 Kb
330	EVSZ (dextral strike–slip top to SE)	-	Greenschist stage	S3	300–400 °C; 2–3 Kb
340	Laurussia–Gondwana transpressional event (top to SE)	-	Granulite to amphibolitic stage	S2	650–750 °C and 8–12 Kb; 550–740 °C and 3–7 Kb
350	Laurussia–Gondwana transpressional event (top to SE)	-	Granulite to amphibolitic stage	S2	650–750 °C and 8–12 Kb; 550–740 °C and 3–7 Kb
360	Laurussia–Gondwana transpressional event (top to SE)	-	Granulite to amphibolitic stage	S2	650–750 °C and 8–12 Kb; 550–740 °C and 3–7 Kb

The D2 event, associated with the syn-kinematic NE–SW-oriented S2 schistosity, is recognizable exclusively within the Old Gneiss Complex (OGC). S2 is linked to a metamorphic evolution (M2), ranging from granulitic to amphibolitic facies. Kinematic indicators on the XZ plane associated with S2 reveal a top-to-SE shear component. The NE–SW-oriented D2 event is dated between 360 Ma and 344 Ma. The causes of the event are attributable to the transpression during the collision between Gondwana and Laurussia.

Between 330 Ma and 315 Ma, the OGC underwent a new deformative event (D3), which primarily affected high-temperature paraderivatives, such as paragneiss and biotitic gneiss, while orthoderivatives, basic rocks, and certain paraderivatives (e.g., quartzites and calcsilicate nodules) tended to preserve their original structures associated with OGC, resulting in the formation of the New Gneiss Complex (NGC; Bt-bearing augen gneiss with pods of OGC lithotypes). This lithotype exhibits a syn-kinematic mylonitic schistosity (S3) and M3 metamorphism in greenschist facies conditions at an age of 325 Ma to 315 Ma, as evidenced by the presence of syn-tectonic Capo Ferro granite. Event D3 is oriented NW–SE and is associated with dextral shear, although, locally, a younger sinistral shear component may be identifiable.

The causes of the D3 event are attributable to the East Variscan Shear Zone (EVSZ), which underwent two episodes of shearing: (i) an older dextral shear event dated at

325 ± 1.3 Ma and characterized by greenschist facies metamorphism [7]; (ii) a younger/local sinistral shear stage with greenschist facies metamorphism, contemporaneous with the synkinematic emplacement of peraluminous granitoid rocks, dated between 318 ± 3 Ma and 315 ± 2 Ma (Capo Ferro Granite [7]). The younger sinistral sense of shear, only observed locally in the Capo Ferro, Sos Aranzos, and Punta de li Tulchi areas, is characterized by tension gashes or σ-type porphyroclasts. The simultaneous presence of oblate and prolate ellipsoids along the S3 foliation suggests a wrench-dominated transpression regime, where the instantaneous strain is indicative of transcurrent movement, while the finite strain reflects contractional deformation [28].

In the Punta Orvili area, the relationships between the D3 event and the E-W-oriented dextral Posada Valley strike–slip Shear Zone (PVSZ) are observable, characterized by the intersection of thin Posada Valley shear zones cutting across S3. These relationships are uniquely observable within this specific outcrop, primarily because the Oligocene–Aquitanian strike–slip tectonic activity obliterated these structures in other areas of Sardinia [66]. Despite the limited extent of the outcrop, ref. [67] highlighted how within it, events characteristic of both the OGC (D2, S2, and M2) and the NGC (D3, S3, and M3) can be identified. The geometric overlap of the fault structures indicates a subsequent event linked to the PVSZ.

The PVSZ is intruded by late Variscan granites dated between 300 Ma and 290 Ma; hence, the appearance of the PVSZ, despite the absence of geochronological data, likely occurred between 310 Ma and 300 Ma.

Correlations between the NGC and the Variscan Morocco, Corsica, Maures, and Argentera Massifs

According to [9], the EVSZ could potentially extend spatially as far as the Moroccan Meseta segment. In fact, [5,26,68,69] outline that the Variscan segment outcropping in southwestern Spain and southern Portugal represents the closest part of the European Variscides to the Moroccan Meseta segment. Both segments are attributed to the "southwestern" branch of the Variscan Belt, accreted either directly to northwestern Gondwana (Morocco) or to the Cantabrian–South Sardinia salient of Gondwana, forming the core of the Ibero-Armorican Arc.

Ref. [70] delineates various regional-scale wrenching shear zones from the late Carboniferous to Permian periods across the Hercynian Meseta orogenic segment, including the anastomosing Hajjar Shear Zone. This shear zone is characterized by a regional transpressive right-lateral NE-trending feature and by a syn- to post-metamorphic ductile to brittle shear. These structural features could be correlated with the dynamics observed by the authors of this paper in the HGMC (High-Grade Metamorphic Complex).

Ref. [71], in the Moroccan Eastern High-Atlas, delineate two structural domains: (i) the Northern Domain (NSD), characterized primarily by N–S Eovariscan polyphased structures (D1 and D2) overprinted by an E–W D3 deformation attributed to a late Carboniferous phase; and (ii) the Central–Southern Domain (CSD), which is only deformed by D3 and exhibits a typical S–C structure developed during this phase, within a principal ductile–brittle shear zone, at a large scale. This D3 event exhibits structural characteristics and geometric overlap similar to those observed for the D2 and D3 events described in this paper.

Refs. [6,9] have highlighted how the late Carboniferous regional shearing process, represented by the East Variscan Shear Zone (EVSZ), affected many Variscan outcrops across western European regions. The EVSZ, documented as a dextral strike–slip shear zone in the literature, extends from the external massifs of the Alps to the Variscan Massifs of Corsica and Sardinia, traversing through the Maures-Tanneron Massif [9,28]. Several key features characterize the EVSZ [6]: it developed during the time span of 325–310 Ma under a transpressional tectonic regime; it exhibited an N–S orientation and displayed dextral transcurrent kinematics consistent with a regional NE–SW direction of shortening; it generated a Riedel system and was often associated with the emplacement of synkinematic "S-Type" granitoids; and it facilitated the exhumation of high-temperature (HT) metamorphic rocks through telescoping processes. The effects of the EVSZ in this area exhibit the same evolutionary characteristics as those described in the HGMC.

In Western Corsica, remnants of pre-batholitic lithological and metamorphic assemblages are preserved as kilometer-scale septa enclosed within lower Carboniferous to early Permian plutons [21,72]. Within the Zicavo [73], Porto-Vecchio, Solenzara-Fautea, Belgodere, and Topiti septa, a ductile shearing event (D1) occurred with a top-to-the-SW direction concurrently with amphibolite facies metamorphism around 360 Ma [74], contributing to crustal thickening. This main event was antedated by eclogite and granulite facies metamorphic events dated to approximately 345–330 Ma [74], preserved as restites within migmatites. After, a ductile shearing event (D2) with a top-to-the-SE direction occurred alongside crustal melting, facilitating the exhumation of the D1 event [75]. In the Zicavo [73], Porto Vecchio, and Belgodre areas, lithotypes exhibiting characteristics akin to those of the Old Gneiss Complex (OGC) in the High-Grade Metamorphic Complex of NE Sardinia have been reported (see Figures 4, 7, and 12 in [21]). The D2 event described by [21] with top-to-the-SE ductile shearing can be correlated to the HGMC D2 event described by authors in this paper. The Belgodère septum experienced a polyphase structural and metamorphic evolution, featuring an early HP event with unknown kinematics, followed by an MP/MT (amphibolite facies) retrogression [62,76,77] coinciding with E-directed shearing, which may correlate with the HGMC NW–SE dextral sense of shear event (D3) described in this paper.

Refs. [11,78] documented the presence of the Camarat Granitic Complex (CGC, 304.5 ± 3.3 Ma [79]) within the migmatitic Internal Zone of the Maures–Tanneron Massif. This complex exhibits highly mylonitized migmatitic gneiss, displaying sinistral shearing and S–C structures indicative of dextral shearing (see Figure 4b in [11]). The gneissic foliation within the continental rocks of the CGC primarily trends NNE–SSW, with moderate to steep dips [11]. Deformation within the migmatitic gneisses is highly heterogeneous and localized along several strike–slip shear zones, which are concordant with the gneissic foliation and correspond to D3 structures. The mylonitic event observed in the CGC could be correlated with the D3 event described in this paper. Furthermore, the emplacement of the CGC might be slightly older than the Capo Ferro Granite (325 ± 1.3 Ma [7]).

Ref. [80] correlated the Argentera Massif with the Mauri-Tanneron Massif, emphasizing similar tectono-metamorphic evolutions both Variscan and pre-Variscan. Ref. [36] identified a steeply dipping kilometer-scale shear zone, the Ferriere-Mollières shear zone (FMSZ), in the Argentera Massif (Western Alps). The predominant structure in the FMSZ is an NW–SE penetrative mylonitic foliation (Sm) associated with well-developed mineral lineation (Lm) primarily defined by Qz and Fsp and subordinately by Sil. A relict tectonic foliation (Sp-1) has been identified in the migmatite complexes constituting the wall-rocks of the shear zone. The mylonitic foliation (Sm) experienced post-shearing gentle folding (Fm + 1) with sub-horizontal axial planes, likely related to post-tectonic collapse. Refs. [36,81], describe the mylonitic lithotypes associated with the FMSZ, highlighting the presence of protomylonites, mylonites, and ultramylonites (Figure 3 in [36,81]), which exhibit textural characteristics similar to those observed for the NGC in NE Sardinia.

It is also essential to consider the geodynamic evolution of the Sardinia–Corsica–Calabria system. Refs. [8,11] have highlighted a system of both counterclockwise and clockwise rotations of the Sardinia–Corsica–Calabria block since the upper Carboniferous to the Oligocene–Miocene period. Ref. [8] used paleomagnetic data to demonstrate that the orientation of the Sardinian–Corsican–Calabrian block shifted from an E–W direction between 360 and 300 Ma (Carboniferous) to an NE–SW direction between 300 and 260 Ma (Permian), following a clockwise rotation of 90 degrees. The Oligocene–Miocene anticlockwise rotation [11,82,83] resulted in the current north–south position of the Corsican–Sardinian block.

7. Conclusions

The Variscan Sardinian High-Grade Metamorphic Complex (HGMC) comprises two metamorphic complexes: the Old Gneiss Complex (OGC) and the New Gneiss Complex (NGC). The OGC is characterized by high-temperature (HT) lithotypes with metamorphic paragenesis ranging from granulitic to amphibolitic facies (350–344 Ma). It exhibits

a secondary penetrative foliation (S2, Figure 13), oriented NE–SW, with an associated top-to-SE sense of shear. The NE–SW structuring of the OGC can be traced back to the Late Devonian (?)-middle Carboniferous evolution. During the D2 event, the rocks of granulitic–amphibolite facies (M2) underwent a telescoping process associated with transpression during the collision between Gondwana and Laurussia.
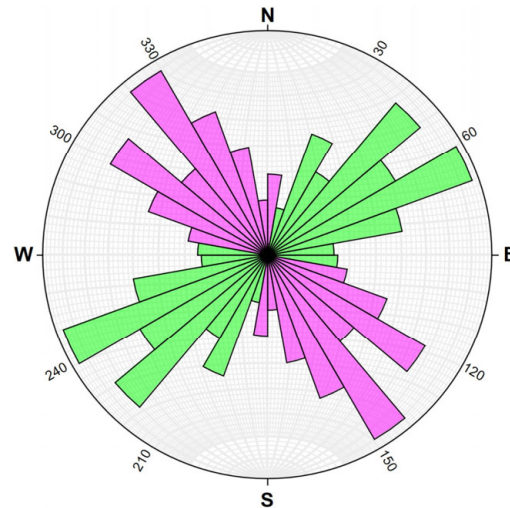

Figure 13. Rose diagram (equal area, lower hemisphere) of 305 S2 planes of OGC (green petals) and of 390 S3 planes in the NGC (pink petals).

The New Gneiss Complex (NGC) is characterized by Bt-bearing augen gneiss, which are sometimes ultramylonitic, with inside pods of lithotypes belonging to OGC that preserve the metamorphic and structural characteristic of the previous tectonometamorphic event (D2, S2, and M2). The NGC is associated with a secondary NW–SE penetrative foliation (S3, Figure 13) under metamorphic conditions of greenschist facies (325–315 Ma) that do not affect the OGC pods within it. The formation of the NGC is attributable to the East Variscan Shear Zone (EVSZ), an intracontinental dextral strike–slip shear zone.

The presence of remnants of the OGC within the NGC, which retain evidence of previous events, and the clear structural and metamorphic relationships and characteristics, strongly suggest that the EVSZ leads to the dismemberment of the OGC into kilometer-scale (e.g., Morungiu Nieddu, Monte Plebi, and San Teodoro areas) to centimeter-scale pods (e.g., the Pittolongu area). The authors therefore suggest considering the entire HGMC as a medium-temperature Regional Mylonitic Complex (RMC) (RMC, Figure 14).

The mylonitic structures and patterns observed in the EVSZ are also present in other surrounding Variscan areas, including Morocco, Corsica, the Maures-Tanneron Massif, and the Argentera. Therefore, the Regional Mylonitic Complex (RMC) associated with this intracontinental shear zone could extend to these regions as well. Our reconstruction is in agreement with the model proposed by [84]. The authors propose a model characterized by magmatic structures distributed along the southern margin of the Variscan Belt during the late Carboniferous period, necessitating the presence of a broad, 1500–3000-kilometer-long network of lithosphere-scale shear zones. Such a structure can account for the intricate rotation paths reconstructed for the southern Variscides and the scattered crystalline massifs along the Alpine chain. Additionally, it offers a coherent explanation for the high-temperature metamorphism and anatexis during the displacement of paleo-Europe relative to Gondwana.

Therefore, taking into consideration the rotations undergone by the Corsica–Sardinia system, the present directions of the NE–SW D2 event and of the NW–SE D3 event would be rotated back to their original positions at the Permian [8,83,85–87]. This would result in the directions becoming NW–SE for the D2 event, with a top-to-NE component of shear, and NE–SW for the D3 event. However, at 360 Ma, the directions would be for the D2 event NW–SE with a shear component top-to-NE, and, for the D3 event, NE–SW (Figure 15).
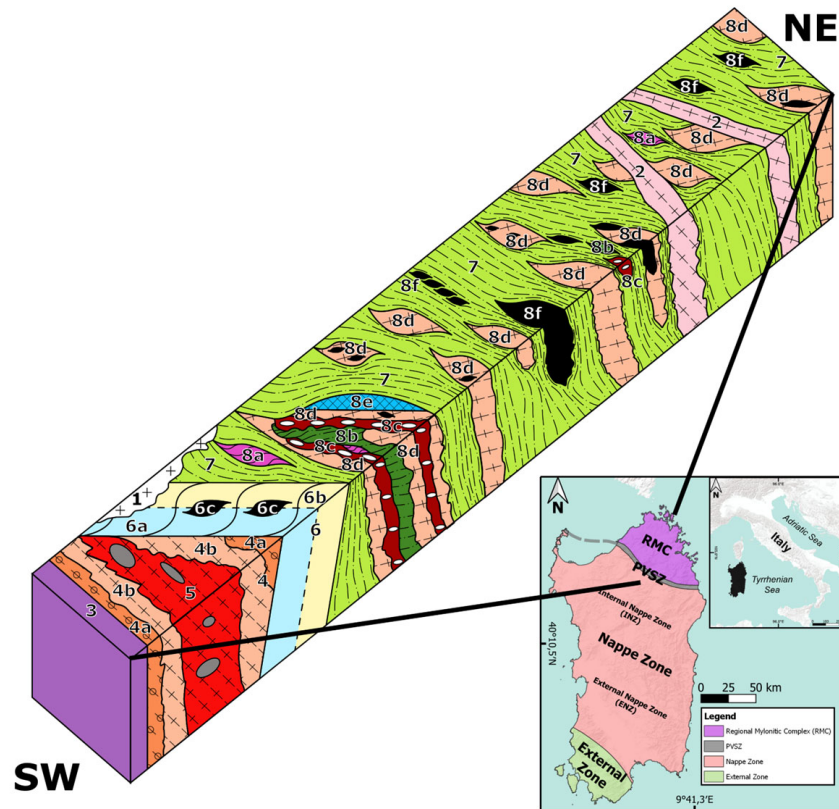
Figure 14. Hypothetical sketch of the Regional Mylonitic Complex (RMC); (1) P.ta Teppilora late granite (300 Ma); (2) Cala Spada and Barrabisa foliated granitoids (325–315 ma); (3) Santa Lucia metamorphic complex (micaschists, paragneiss, marble, and quartzites in the Ab + Grt zone; (4) Lodè-Mamone Ordovician metavolcanic complex: (4a) ryoilitic augen gneiss and (4b) leucocratic orthogneiss and metaplites; (5) Riu Mannu Ordovician orthogneiss with coeval thermometamorphic lithoptypes (And + Bt-bearing cornubianites and Grs + Cpx + Ves + Wo-bearing calcsilicates); (6) Posada Valley Shear Zone (dextral strike–slip shear zone): (6a) Punta Gortomedda metamorphic complex (micaschists, paragneiss, quartzites, and marble in the St + Grt + Bt zone), (6b) Bruncu Nieddu metamorphic complex (micaschists, paragneiss, quartzites, orthoderivates, and marble in the Ky + Grt + Bt zone and ultramylonites of Pedra Su Gattu), and (6c) amphibolites of P.ta Figliacoro; (7) New Gneiss Complex (NGC) mylonitic/ultramylnitic Bt-bearing augen gneiss; (8) Old Gneiss Complex (OGC): (8a) Punta Nidu e Corvu Sil + Ms-bearing gneiss, (8b) Punta dell'Ainu Sil + Ms-bearing paragneiss, (8c) Punta S.Anna-Brunella metamorphic complex (paragneiss with calcsilicates nodules, gneiss, and Tamarispa calcsilicates), (8d) Ordovician orthogneisses (San Lorenzo-Tanaunella, Straulas, Punta de li Tulchi, P.ta Tittinosu, Monte Plebi Leptino Amphibolitic Complex, Pittolongu, Punta Bados-Cala Serenella, Diga del Liscia, Golfo Aranci, Palau, Punta Falcone), (8e) San Teodoro metamorphic complex (stromatitic gneiss, nebulites and migmatitic gneiss), (8f) metabasites (Punta Orvili, Pittolongu, and Sos Aranzos-Punta Bados amphibolites; Punta de li Tulchi, Golfo Aranci, and Golfo di Cugnaga amphibolitized eclogites; Morungiu Nieddu amphibolitized granulites).

The East Variscan Shear Zone (EVSZ) can be regarded as one of the most significant southern alignments during the Carboniferous interaction/convergence between the Gondwana and Laurussia plates. It was coeval with numerous regional shear zones leading to an indentation between Gondwana and Laurussia, with sectors experiencing a frontal collision (French Massif Central and Vosges Massif) coeval with others experiencing an oblique collision.
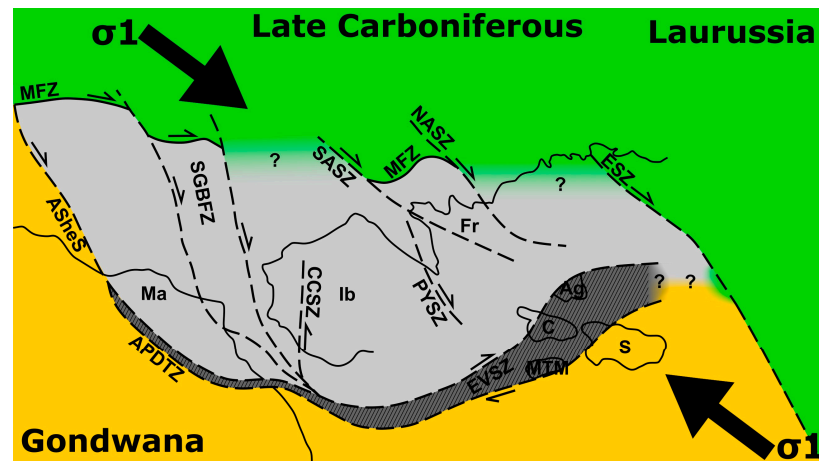
Figure 15. Sketch of the northern boundary of Gondwana and its relationships with Laurussia in the late Carboniferous period; C: Corsica; Fr: France; Ib: Iberia; Ma: Morocco; S: Sardinia; Ag: Argentera Massif; APDTZ: Atlas Palaeozoic Dextral Transform Zone; ASheS: Atlas shear system; CCSZ: Coimbra–Cordoba Shear Zone; ESZ: Elbe Shear Zone; EVSZ: East Variscan Shear Zone; MFZ: Minas Fault Zone; MTM: Maures-Tanneron Massif; NASZ: north Armorican Shear Zone; PySZ: Pyrenees Shear Zone; SASZ: South Armorican Shear Zone; SGBF: Southern Grand Banks Fault; striped dark grey: Regional Mylonitic Complex (RMC); light grey: Gondwana-Derived Continent (GDC) (modified from [7]; the Sardinia–Corsica block is positioned according to [8,83,85–87]).

Author Contributions: Conceptualization, F.M. and F.M.E.; methodology, F.M. and F.M.E.; software, F.M.; validation, F.M.E.; formal analysis, F.M.; investigation, F.M. and F.M.E.; resources, F.M.E.; data curation, F.M. and F.M.E.; writing—original draft preparation, F.M. and F.M.E.; writing—review and editing, F.M. and F.M.E.; visualization, F.M. and F.M.E.; supervision, F.M.E.; project administration, F.M.E.; funding acquisition, F.M. and F.M.E. All authors have read and agreed to the published version of the manuscript.

Data Availability Statement: All the data are presented in the paper.

Conflicts of Interest: The authors declare no conflicts of interest.

References

1. Matte, P. The Variscan Collage and Orogeny (480–290 Ma) and the Tectonic Definition of the Armorica Microplate: A Review. *Terra Nova* **2001**, *13*, 122–128. [CrossRef]
2. Stampfli, G.M.; Borel, G.D. A Plate Tectonic Model for the Paleozoic and Mesozoic Constrained by Dynamic Plate Boundaries and Restored Synthetic Oceanic Isochrons. *Earth Planet. Sci. Lett.* **2002**, *196*, 17–33. [CrossRef]
3. Stampfli, G.M.; Kozur, H.W. Europe from the Variscan to the Alpine Cycles. In *European Lithosphere Dynamics*; Gee, D.G., Stephenson, R.A., Eds.; Geological Society of London: London, UK, 2006; Volume 32, ISBN 978-1-86239-212-0.
4. Von Raumer, J.F.; Bussy, F.; Stampfli, G.M. The Variscan Evolution in the External Massifs of the Alps and Place in Their Variscan Framework. *Comptes Rendus Geosci.* **2009**, *341*, 239–252. [CrossRef]
5. Michard, A.; Soulaimani, A.; Hoepffner, C.; Ouanaimi, H.; Baidder, L.; Rjimati, E.C.; Saddiqi, O. The South-Western Branch of the Variscan Belt: Evidence from Morocco. *Tectonophysics* **2010**, *492*, 1–24. [CrossRef]
6. Padovano, M.; Elter, F.M.; Pandeli, E.; Franceschelli, M. The East Variscan Shear Zone: New Insights into Its Role in the Late Carboniferous Collision in Southern Europe. *Int. Geol. Rev.* **2012**, *54*, 957–970. [CrossRef]
7. Padovano, M.; Dörr, W.; Elter, F.M.; Gerdes, A. The East Variscan Shear Zone: Geochronological Constraints from the Capo Ferro Area (NE Sardinia, Italy). *Lithos* **2014**, *196–197*, 27–41. [CrossRef]
8. Edel, J.B.; Schulmann, K.; Lexa, O.; Lardeaux, J.M. Late Palaeozoic Palaeomagnetic and Tectonic Constraints for Amalgamation of Pangea Supercontinent in the European Variscan Belt. *Earth-Sci. Rev.* **2018**, *177*, 589–612. [CrossRef]
9. Elter, F.M.; Gaggero, L.; Mantovani, F.; Pandeli, E.; Costamagna, L.G. The Atlas-East Variscan -Elbe Shear System and Its Role in the Formation of the Pull-Apart Late Palaeozoic Basins. *Int. J. Earth Sci.* **2020**, *109*, 739–760. [CrossRef]

10. Martínez Catalán, J.R.; Schulmann, K.; Ghienne, J.-F. The Mid-Variscan Allochthon: Keys from Correlation, Partial Retrodeformation and Plate-Tectonic Reconstruction to Unlock the Geometry of a Non-Cylindrical Belt. *Earth-Sci. Rev.* **2021**, *220*, 103700. [CrossRef]

11. Bolle, O.; Corsini, M.; Diot, H.; Laurent, O.; Melis, R. Late-Orogenic Evolution of the Southern European Variscan Belt Constrained by Fabric Analysis and Dating of the Camarat Granitic Complex and Coeval Felsic Dykes (Maures–Tanneron Massif, SE France). *Tectonics* **2023**, *42*, e2022TC007310. [CrossRef]

12. Matte, P. Accretionary History and Crustal Evolution of the Variscan Belt in Western Europe. *Tectonophysics* **1991**, *196*, 309–337. [CrossRef]

13. Schulmann, K.; Edel, J.-B.; Martínez Catalán, J.R.; Mazur, S.; Guy, A.; Lardeaux, J.-M.; Ayarza, P.; Palomeras, I. Tectonic Evolution and Global Crustal Architecture of the European Variscan Belt Constrained by Geophysical Data. *Earth-Sci. Rev.* **2022**, *234*, 104195. [CrossRef]

14. Ábalos, B.; Carreras, J.; Druguet, E.; Viruete, J.E.; Pugnaire, M.T.G.; Alvarez, S.L.; Quesada, C.; Fernández, L.R.R.; Gil-Ibarguchi, J.I. Variscan and Pre-Variscan Tectonics. In *The Geology of Spain*; Gibbons, W., Moreno, T., Eds.; Geological Society of London: London, UK, 2002; ISBN 978-1-86239-127-7.

15. Helbing, H.; Frisch, W.; Bons, P.D. South Variscan Terrane Accretion: Sardinian Constraints on the Intra-Alpine Variscides. *J. Struct. Geol.* **2006**, *28*, 1277–1291. [CrossRef]

16. Festa, V.; Caggianelli, A.; Kruhl, J.H.; Liotta, D.; Prosser, G.; Gueguen, E.; Paglionico, A. Late-Hercynian Shearing during Crystallization of Granitoid Magmas (Sila Massif, Southern Italy): Regional Implications. *Geodin. Acta* **2006**, *19*, 185–195. [CrossRef]

17. Molli, G.; Montanini, A.; Frank, W. Morb-Derived Variscan Amphibolites in the Northern Apennine Basement: The Cerreto Metamorphic Slices (Tuscan-Emilian Apennine, Nw Italy). *Ofioliti* **2002**, *27*, 17–30. [CrossRef]

18. Von Raumer, J.F.; Stampfli, G.M.; Bussy, F. Gondwana-Derived Microcontinents—The Constituents of the Variscan and Alpine Collisional Orogens. *Tectonophysics* **2003**, *365*, 7–22. [CrossRef]

19. Torsvik, T.H.; Cocks, L.R.M. Gondwana from Top to Base in Space and Time. *Gondwana Res.* **2013**, *24*, 999–1030. [CrossRef]

20. Corsini, M.; Rolland, Y. Late Evolution of the Southern European Variscan Belt: Exhumation of the Lower Crust in a Context of Oblique Convergence. *C. R. Géosci.* **2009**, *341*, 214–223. [CrossRef]

21. Faure, M.; Rossi, P.; Gaché, J.; Melleton, J.; Frei, D.; Li, X.; Lin, W. Variscan Orogeny in Corsica: New Structural and Geochronological Insights, and Its Place in the Variscan Geodynamic Framework. *Int. J. Earth Sci.* **2014**, *103*, 1533–1551. [CrossRef]

22. Gutiérrez-Alonso, G.; Fernández-Suárez, J.; Weil, A.B.; Brendan Murphy, J.; Damian Nance, R.; Corfú, F.; Johnston, S.T. Self-Subduction of the Pangaean Global Plate. *Nat. Geosci.* **2008**, *1*, 549–553. [CrossRef]

23. Ballèvre, M.; Manzotti, P.; Dal Piaz, G.V. Pre-Alpine (Variscan) Inheritance: A Key for the Location of the Future Valaisan Basin (Western Alps). *Tectonics* **2018**, *37*, 786–817. [CrossRef]

24. Weil, A.B.; Gutiérrez-Alonso, G.; Johnston, S.T.; Pastor-Galán, D. Kinematic Constraints on Buckling a Lithospheric-Scale Orocline along the Northern Margin of Gondwana: A Geologic Synthesis. *Tectonophysics* **2013**, *582*, 25–49. [CrossRef]

25. Martínez Catalán, J.R. Are the Oroclines of the Variscan Belt Related to Late Variscan Strike-Slip Tectonics? *Terra Nova* **2011**, *23*, 241–247. [CrossRef]

26. Dias, R.; Hadani, M.; Leal Machado, I.; Adnane, N.; Hendaq, Y.; Madih, K.; Matos, C. Variscan Structural Evolution of the Western High Atlas and the Haouz Plain (Morocco). *J. Afr. Earth Sci.* **2011**, *61*, 331–342. [CrossRef]

27. Neubauer, F.; Handler, R. Variscan Orogeny in the Eastern Alps and Bohemian Massif: How Do These Units Correlate. *Mitt. Österr. Geol. Ges.* **2000**, *92*, 35–59.

28. Elter, F.M.; Padovano, M.; Kraus, R.K. The Emplacement of Variscan HT Metamorphic Rocks Linked to the Interaction between Gondwana and Laurussia: Structural Constraints in NE Sardinia (Italy). *Terra Nova* **2010**, *22*, 369–377. [CrossRef]

29. Carosi, R.; Frassi, C.; Montomoli, C. Deformation during Exhumation of Medium- and High-Grade Metamorphic Rocks in the Variscan Chain in Northern Sardinia (Italy). *Geol. J.* **2009**, *44*, 280–305. [CrossRef]

30. Cruciani, G.; Montomoli, C.; Carosi, R.; Franceschelli, M.; Puxeddu, M. Continental Collision from Two Perspectives: A Review of Variscan Metamorphism and Deformation in Northern Sardinia. *Period. Mineral.* **2015**, *84*, 657–699. [CrossRef]

31. Franceschelli, M.; Puxeddu, M.; Cruciani, G. Variscan Metamorphism in Sardinia, Italy: Review and Discussion. *J. Virtual Explor.* **2005**, *19*, 2–36. [CrossRef]

32. Costamagna, L.G.; Elter, F.M.; Gaggero, L.; Mantovani, F. Contact Metamorphism in Middle Ordovician Arc Rocks (SW Sardinia, Italy): New Paleogeographic Constraints. *Lithos* **2016**, *264*, 577–593. [CrossRef]

33. Conti, P.; Carmignani, L.; Funedda, A. Change of Nappe Transport Direction during the Variscan Collisional Evolution of Central-Southern Sardinia (Italy). *Tectonophysics* **2001**, *332*, 255–273. [CrossRef]

34. Carosi, R.; Palmeri, R. Orogen-Parallel Tectonic Transport in the Variscan Belt of Northeastern Sardinia (Italy): Implications for the Exhumation of Medium-Pressure Metamorphic Rocks. *Geol. Mag.* **2002**, *139*, 497–511. [CrossRef]

35. Helbing, H.; Tiepolo, M. Age Determination of Ordovician Magmatism in NE Sardinia and Its Bearing on Variscan Basement Evolution. *J. Geol. Soc.* **2005**, *162*, 689–700. [CrossRef]

36. Carosi, R.; D'Addario, E.; Mammoliti, E.; Montomoli, C.; Simonetti, M. Geology of the Northwestern Portion of the Ferriere-Mollieres Shear Zone, Argentera Massif, Italy. *J. Maps* **2016**, *12*, 466–475. [CrossRef]

37. Carosi, R.; Montomoli, C.; Iacopini, D.; Petroccia, A.; Simonetti, M.; Oggiano, G. Geology of the Asinara Island (Sardinia, Italy). *J. Maps* **2024**, *20*, 2317136. [CrossRef]

38. Elter, F.M.; Corsi, B.; Cricca, P.; Muzio, G. The South-Western Alpine Foreland: Correlation between Two Sectors of the Variscan Chain Belonging to "Stable Europe": Sardinia(-)Corsica and the Maures Massif (South-Eastern France). *Geodin. Acta* **2004**, *17*, 31–40. [CrossRef]

39. Corsi, B.; Elter, F.M. Eo-Variscan (Devonian?) Melting in the High Grade Metamorphic Complex of the NE Sardinia Belt (Italy). *Geodin. Acta* **2006**, *19*, 155–164. [CrossRef]

40. Cruciani, G.; Franceschelli, M.; Elter, F.M.; Puxeddu, M.; Utzeri, D. Petrogenesis of Al–Silicate-Bearing Trondhjemitic Migmatites from NE Sardinia, Italy. *Lithos* **2008**, *102*, 554–574. [CrossRef]

41. Elter, F.M.; Musumeci, G.; Pertusati, P.C. Late Hercynian Shear Zones in Sardinia. *Tectonophysics* **1990**, *176*, 387–404. [CrossRef]

42. Elter, F.M.; Faure, M.; Ghezzo, C.; Corsi, B. Late Hercynian Shear Zones in Northeastern Sardinia (Italy). *Géologie Fr.* **1999**, *2*, 3–16.

43. Carmignani, L.; Carosi, R.; Di Pisa, A.; Gattiglio, M.; Musumeci, G.; Oggiano, G.; Carlo Pertusati, P. The Hercynian Chain in Sardinia (Italy). *Geodin. Acta* **1994**, *7*, 31–47. [CrossRef]

44. Carmignani, L.; Oggiano, G.; Funedda, A.; Conti, P.; Pasci, S. The Geological Map of Sardinia (Italy) at 1:250,000 Scale. *J. Maps* **2016**, *12*, 826–835. [CrossRef]

45. Carosi, R.; Montomoli, C.; Tiepolo, M.; Frassi, C. Geochronological Constraints on Post-Collisional Shear Zones in the Variscides of Sardinia (Italy). *Terra Nova* **2012**, *24*, 42–51. [CrossRef]

46. Carosi, R.; Montomoli, C.; Iaccarino, S.; Benetti, B.; Petroccia, A.; Simonetti, M. Constraining the Timing of Evolution of Shear Zones in Two Collisional Orogens: Fusing Structural Geology and Geochronology. *Geosciences* **2022**, *12*, 231. [CrossRef]

47. Di Vincenzo, G. The Relationship between Tectono-Metamorphic Evolution and Argon Isotope Records in White Mica: Constraints from in Situ 40Ar-39Ar Laser Analysis of the Variscan Basement of Sardinia. *J. Petrol.* **2004**, *45*, 1013–1043. [CrossRef]

48. Genier, F.; Bussy, F.; Epard, J.-L.; Baumgartner, L. Water-Assisted Migmatization of Metagraywackes in a Variscan Shear Zone, Aiguilles-Rouges Massif, Western Alps. *Lithos* **2008**, *102*, 575–597. [CrossRef]

49. Corsini, M.; Ruffet, G.; Caby, R. Alpine and Late-Hercynian Geochronological Constraints in the Argentera Massif (Western Alps). *Eclogae Geol. Helvetiae* **2004**, *97*, 3–15. [CrossRef]

50. Franceschelli, M.; Columbu, S.; Elter, F.M.; Cruciani, G. Giant Garnet Crystals in Wollastonite–Grossularite–Diopside-Bearing Marbles from Tamarispa (NE Sardinia, Italy): Geosite Potential, Conservation, and Evaluation as Part of a Regional Environmental Resource. *Geoheritage* **2021**, *13*, 96. [CrossRef]

51. Ferrara, G.; Ricci, C.A.; Rita, F. Isotopic Ages and Tectono-Metamorphic History of the Metamorphic Basement of North-Eastern Sardinia. *Contrib. Mineral. Petrol.* **1978**, *68*, 99–106. [CrossRef]

52. Giacomini, F.; Bomparola, R.M.; Ghezzo, C.; Guldbransen, H. The Geodynamic Evolution of the Southern European Variscides: Constraints from the U/Pb Geochronology and Geochemistry of the Lower Palaeozoic Magmatic-Sedimentary Sequences of Sardinia (Italy). *Contrib. Mineral. Petrol.* **2006**, *152*, 19–42. [CrossRef]

53. Cruciani, G.; Franceschelli, M.; Carosi, R.; Montomoli, C. P-T Path from Garnet Zoning in Pelitic Schist from NE Sardinia, Italy: Further Constraints on the Metamorphic and Tectonic Evolution of the North Sardinia Variscan Belt. *Lithos* **2022**, *428–429*, 106836. [CrossRef]

54. Fossen, H.; Cavalcante, G.C.G. Shear Zones—A Review. *Earth-Sci. Rev.* **2017**, *171*, 434–455. [CrossRef]

55. Passchier, C.W.; Trouw, R.A.J. *Microtectonics*; Springer: Berlin/Heidelberg, Germany, 1996; ISBN 978-3-540-64003-5.

56. Cappelli, B.; Liotta, D.; Cocozza, T. Università degli studi di Siena Dipartimento di scienze della Terra. In *Geologia del Basamento Italiano: Convegno in Memoria di Tommaso Cocozza Accademia dei Fisiocritici, Siena, 21–22 Marzo 1991 Abstracts/Coordinamento Editoriale a Cura di Beatrice Cappelli e Domenico Liotta*; Università, Dipartimento di Scienze della Terra: Siena, Italy, 1991.

57. Cruciani, G.; Franceschelli, M.; Scodina, M.; Puxeddu, M. Garnet zoning in kyanite-bearing eclogite from golfo aranci: New data on the early prograde P–T evolution in NE Sardinia, Italy. *Geol. J.* **2019**, *54*, 190–205. [CrossRef]

58. Cruciani, G.; Franceschelli, M.; Groppo, C.; Spano, M.E. Metamorphic Evolution of Non-Equilibrated Granulitized Eclogite from Punta de Li Tulchi (Variscan Sardinia) Determined through Texturally Controlled Thermodynamic Modelling. *J. Metamorph. Geol.* **2012**, *30*, 667–685. [CrossRef]

59. Franceschelli, M.; Eltrudis, A.; Memmi, I.; Palmeri, R.; Carcangiu, G. Multi-Stage Metamorphic Re-Equilibration in Eclogitic Rocks from the Hercynian Basement of NE Sardinia (Italy). *Mineral. Petrol.* **1998**, *62*, 167–193. [CrossRef]

60. Palmeri, R.; Fanning, M.; Franceschelli, M.; Memmi, I.; Ricci, C.A. SHRIMP Dating of Zircons in Eclogite from the Variscan Basement in North-Eastern Sardinia (Italy). *Neues Jahrb. Mineral.—Monatshefte* **2004**, *6*, 275–288. [CrossRef]

61. Cruciani, G.; Franceschelli, M.; Musumeci, G.; Scodina, M. Geology of the Montigiu Nieddu Metamorphic Basement, NE Sardinia (Italy). *J. Maps* **2020**, *16*, 543–551. [CrossRef]

62. Massonne, H.-J.; Cruciani, G.; Franceschelli, M. Geothermobarometry on Anatectic Melts—A High-Pressure Variscan Migmatite from Northeast Sardinia. *Int. Geol. Rev.* **2013**, *55*, 1490–1505. [CrossRef]

63. Mukherjee, S. *Atlas of Shear Zone Structures in Meso-Scale*; Springer Geology; Springer International Publishing: Cham, Switzerland, 2014; ISBN 978-3-319-00088-6.

64. Scodina, M.; Cruciani, G.; Franceschelli, M. Metamorphic Evolution and P–T Path of the Posada Valley Amphibolites: New Insights on the Variscan High Pressure Metamorphism in NE Sardinia, Italy. *C. R. Géosci.* **2021**, *353*, 227–246. [CrossRef]

65. Frassi, C. Structure of the Variscan Metamorphic Complexes in the Central Transect of the Posada-Asinara Line (SW Gallura Region, Northern Sardinia, Italy). *J. Maps* **2015**, *11*, 136–145. [CrossRef]

66. Oggiano, G.; Funedda, A.; Carmignani, L.; Pasci, S. The Sardinia-Corsica Microplate and Its Role in the Northern Apennine Geodynamics: New Insights from the Tertiary Intraplate Strike-Slip Tectonics of Sardinia. *Ital. J. Geosci.* **2009**, *128*, 527–539. [CrossRef]

67. Cruciani, G.; Franceschelli, M.; Iaccarino, S.; Montomoli, C.; Carosi, R.; Scodina, M. P–T Conditions in Mylonitic Gneiss from Posada Shear Zone, NE Sardinia. In Proceedings of the Abstracts del Congresso SIMP-SGI-SOGeI-AIV, Pisa, Italy, 1 January 2017.

68. Hoepffner, C.; Houari, M.R.; Bouabdelli, M. Tectonics of the North African Variscides (Morocco, Western Algeria): An Outline. *C. R. Géosci.* **2006**, *338*, 25–40. [CrossRef]

69. Ait Daoud, M.; Essalhi, A.; Essalhi, M.; Toummite, A. The Role of Variscan Shortening in the Control of Mineralization Deposition in Tadaout-Tizi n'rsas Mining District (Eastern Anti-Atlas, Morocco). *Bull. Miner. Res. Explor.* **2019**, *161*, 13–32. [CrossRef]

70. Admou, S.; Branquet, Y.; Badra, L.; Barbanson, L.; Outhounjite, M.; Khalifa, A.; Zouhair, M.; Maacha, L. The Hajjar Regional Transpressive Shear Zone (Guemassa Massif, Morocco): Consequences on the Deformation of the Base-Metal Massive Sulfide Ore. *Minerals* **2018**, *8*, 435. [CrossRef]

71. Houari, M.-R.; Hoepffner, C. Late Carboniferous Dextral Wrench-Dominated Transpression along the North African Craton Margin (Eastern High-Atlas, Morocco). *J. Afr. Earth Sci.* **2003**, *37*, 11–24. [CrossRef]

72. Rossi, P.; Oggiano, G.; Cocherie, A. A Restored Section of the "Southern Variscan Realm" across the Corsica–Sardinia Microcontinent. *Comptes Rendus Geosci.* **2009**, *341*, 224–238. [CrossRef]

73. Dulcetta, L.; Faure, M.; Rossi, P.; Cruciani, G.; Franceschelli, M. Geology of the Zicavo Metamorphic Complex, Southern Corsica (France). *J. Maps* **2023**, *19*, 2264320. [CrossRef]

74. Li, X.-H.; Faure, M.; Lin, W. From Crustal Anatexis to Mantle Melting in the Variscan Orogen of Corsica (France): SIMS U–Pb Zircon Age Constraints. *Tectonophysics* **2014**, *634*, 19–30. [CrossRef]

75. Cruciani, G.; Franceschelli, M.; Massonne, H.-J.; Musumeci, G. Evidence of Two Metamorphic Cycles Preserved in Garnet from Felsic Granulite in the Southern Variscan Belt of Corsica, France. *Lithos* **2021**, *380–381*, 105919. [CrossRef]

76. Giacomini, F.; Dallai, L.; Carminati, E.; Tiepolo, M.; Ghezzo, C. Exhumation of a Variscan Orogenic Complex: Insights into the Composite Granulitic–Amphibolitic Metamorphic Basement of South-East Corsica (France). *J. Metamorph. Geol.* **2008**, *26*, 403–436. [CrossRef]

77. Paquette, J.-L.; Ménot, R.-P.; Pin, C.; Orsini, J.-B. Episodic and Short-Lived Granitic Pulses in a Post-Collisional Setting: Evidence from Precise U–Pb Zircon Dating through a Crustal Cross-Section in Corsica. *Chem. Geol.* **2003**, *198*, 1–20. [CrossRef]

78. Bellot, J.-P. The Palaeozoic Evolution of the Maures Massif (France) and Its Potential Correlation with Others Areas of the Variscan Belt: A Review. *J. Virtual Explor.* **2005**, *19*, 1–23. [CrossRef]

79. Morillon, A.-C.; Féraud, G.; Sosson, M.; Ruffet, G.; Crevola, G.; Lerouge, G. Diachronous Cooling on Both Sides of a Major Strike Slip Fault in the Variscan Maures Massif (South-East France), as Deduced from a Detailed 40Ar/39Ar Study. *Tectonophysics* **2000**, *321*, 103–126. [CrossRef]

80. Compagnoni, R.; Ferrando, S.; Lombardo, B.; Radulesco, N.; Rubatto, D. Paleo-European Crust of the Italian Western Alps: Geological History of the Argentera Massif and Comparison with Mont Blanc-Aiguilles Rouges and Maures-Tanneron Massifs. *J. Virtual Explor.* **2010**, *36*, 1–30. [CrossRef]

81. Simonetti, M.; Carosi, R.; Montomoli, C.; Langone, A.; D'Addario, E.; Mammoliti, E. Kinematic and Geochronological Constraints on Shear Deformation in the Ferriere-Mollières Shear Zone (Argentera-Mercantour Massif, Western Alps): Implications for the Evolution of the Southern European Variscan Belt. *Int. J. Earth Sci.* **2018**, *107*, 2163–2189. [CrossRef]

82. Mantovani, F.; Elter, F.M.; Pandeli, E.; Briguglio, A.; Piazza, M. The Portofino Conglomerate (Eastern Liguria, Northern Italy): Provenance, Age and Geodynamic Implications. *Geosciences* **2023**, *13*, 154. [CrossRef]

83. Edel, J.; Dubois, D.; Marchant, R.; Hernandez, J.; Cosca, M. La Rotation Miocène Inférieur Du Bloc Corso-Sarde. Nouvelles Contraintes Paléomagnétiques Sur La Fin Du Mouvement. *Bull. Soc. Geol. Fr.* **2001**, *172*, 275–283. [CrossRef]

84. Casini, L.; Cuccuru, S.; Puccini, A.; Oggiano, G.; Rossi, P. Evolution of the Corsica–Sardinia Batholith and Late-Orogenic Shearing of the Variscides. *Tectonophysics* **2015**, *646*, 65–78. [CrossRef]

85. Edel, J.-B.; Schulmann, K.; Lexa, O.; Diraison, M.; Géraud, Y. Permian Clockwise Rotations of the Ebro and Corso-Sardinian Blocks during Iberian–Armorican Oroclinal Bending: Preliminary Paleomagnetic Data from the Catalan Coastal Range (NE Spain). *Tectonophysics* **2015**, *657*, 172–186. [CrossRef]

86. Edel, J.-B.; Casini, L.; Oggiano, G.; Rossi, P.; Schulmann, K. Early Permian 90° Clockwise Rotation of the Maures–Estérel–Corsica–Sardinia Block Confirmed by New Palaeomagnetic Data and Followed by a Triassic 60° Clockwise Rotation. *Geol. Soc. Lond. Spec. Publ.* **2014**, *405*, 333–361. [CrossRef]

87. Edel, J.B. The Rotations of the Variscides during the Carboniferous Collision: Paleomagnetic Constraints from the Vosges and the Massif Central (France). *Tectonophysics* **2001**, *332*, 69–92. [CrossRef]